

Dual-mode blue emission, paramagnetic properties of Yb^{3+} - Tm^{3+} co-doped GdOCl difunctional nanostructures

Juan Chen¹ · Yan Song¹ · Dan Li¹ · Qianli Ma¹ · Xiangting Dong¹  · Wensheng Yu¹ · Ying Yang¹ · Jinxian Wang¹ · Guixia Liu¹ · Tingting Wang¹

Received: 13 August 2017 / Accepted: 1 September 2017 / Published online: 8 September 2017
© Springer Science+Business Media, LLC 2017

Abstract A series of $\text{GdOCl}:\text{Yb}^{3+}, \text{Tm}^{3+}$ one-dimensional nanostructures with dual-mode [down-conversion (DC) and up-conversion (UC)] luminescence were successfully fabricated by electrospinning technique incorporated with double-crucible chlorination method. The samples have single-phase tetragonal structure with space group of $P4/nmm$. The diameter and width of $\text{GdOCl}:10\% \text{Yb}^{3+}, 0.1\% \text{Tm}^{3+}$ nanofibers and nanobelts are 212.84 ± 1.04 nm and 1.07 ± 0.03 μm , respectively. Excited by 357-nm ultraviolet (UV) light and 980-nm near-infrared (NIR) light, Yb^{3+} and Tm^{3+} ions co-doped GdOCl nanostructures exhibit bright blue emission. The mechanism of UC emission is determined to be three-photon process. The energy transfer processes from Yb^{3+} to Tm^{3+} are discussed in detail. Moreover, the as-obtained products possess paramagnetic properties at ambient temperature. The type of difunctional one-dimensional nanomaterials has promising applications in anti-counterfeiting, drug delivery, solid state lasers, biolabels and light emitting diodes (LEDs).

1 Introduction

Lanthanide oxyhalides have aroused extensive surveys for applications in field-emission driven phosphors, up-conversion (UC) lasers, optical telecommunications infrastructure, biosensing, medical diagnosis, photocatalytic activity and bioimaging probes [1–7]. Lanthanide oxychlorides have

been researched for catalytic utilizations in ethane oxidative dehydrogenation, methane coupling and for gas sensor applications [8]. When doped with activator ions, these nanomaterials reveal favorable down-conversion (DC) and UC luminescence. GdOCl , by virtue of the multitudinous superiority of lanthanide oxyhalides, is a well-suited substrate of phosphor doped with the suitable rare earth dopant [9]. GdOCl employs a tetragonal matlockite PbFCl structure with space group of $P4/nmm$, thereinto, cationic layers of GdO^+ and anionic layers of Cl^- alternating change in the direction of crystallization [10]. Nanofibers and nanobelts are new-fashioned varieties of one-dimensional (1D) nanostructures possessing unique morphologies. The 1D nanostructures of rare earth doped nanomaterials have attracted enormous attention in recent years [11–13]. Tailoring of aspect ratio in rare earth based 1D nanostructures offer several advantages, for instance, quantum confinement, tunable electrical, magnetic, and optical properties [14]. Thus far, some synthetic approaches have been reported for the fabrication of LnOCl nanomaterials, such as hydrothermal syntheses, mechanochemical grinding, chloride salt-assisted method, solid-state reaction method and thermohydrolysis [15–19]. Although these preparative processes are assuredly successful in the synthesis of nanoscale lanthanide oxychlorides, they induce barely little selectivity with concerning to size, morphology, or the directions of crystallographic growth, resulting in generation of polydisperse nanopowders. Electrospinning is an ordinary, advantageous, straightforward and universal technique for fabricating long fibers [20, 21], such as rare earth fluoride nanofibers [22], rare earth oxide nanofibers [23, 24], rare earth oxyfluoride nanofibers [25], hollow nanofibers [26], core-shell structured coaxial nanofibers [27], and nanobelts [28], etc.

Recently, rare earth ions (RE^{3+}) doped luminescent nanomaterials have already gained comprehensive researches

✉ Xiangting Dong
dongxiangting888@163.com

¹ Key Laboratory of Applied Chemistry and Nanotechnology at Universities of Jilin Province, Changchun University of Science and Technology, Changchun 130022, China

owing to their unique 4f electron configuration and specific properties. RE-doped luminescent nanomaterials have been extensively applied in plasma flat panel displays (PDP), fluorescent lamps, field emission display (FEDs) and white LEDs [29–32]. The characteristic transition of luminescent materials determines the color purity of emission. Although rich levels of lanthanide ions give its multispectral emitting, but Tm^{3+} ions only generates around 458 nm blue light under the near ultraviolet excitation, it provides a high color purity of blue light emission. Tm^{3+} ions not only could possess own DC emission but also exhibit UC properties, manifesting as dividing one high energy photon into two or more lower energy photons. The UC is due to its excellent light-emitting properties such as high brightness, low-energy, low-cost and high efficiency [33–35]. It is well-known that Tm^{3+} is one of the most crucial activator ion in the UC luminescent RE ions, which can reveal prominent blue ($^1\text{G}_4 \rightarrow ^3\text{H}_6$) and weak red ($^1\text{G}_4 \rightarrow ^3\text{F}_4$ and $^3\text{F}_3 \rightarrow ^3\text{H}_6$) emission under the excitation of a 980 nm diode laser, and Yb^{3+} ion is a good sensitizer for Tm^{3+} [36]. Therefore, the Yb^{3+} – Tm^{3+} couple extremely improve UC luminescent efficiency via energy transfer due to the strong absorption at 980 nm, likewise it can be used to generate visible blue UC emission [37]. Gadolinium ions (Gd^{3+}) have seven unpaired 4f electrons which populate electron orbitals with the same direction in a half full state according to the lowest energy principle. Thus, Gd-based materials possess a large magnetic moment and magnetism can be easily induced by the magnetic fields [38–40]. Therefore, Gd^{3+} -based oxychlorides are good candidates as dual-mode luminescent materials, namely, optical imaging nanoprobe and magnetic resonance image (MRI) contrast agents. Up to now, some groups synthesized the dual-mode luminescent and multifunctional Ln^{3+} ions doped NaGdF_4 nanocrystals [41], NaGdF_4 nanoparticles [42, 43] and BaGdF_5 nanoparticles [44]. However, the dual-mode emission of the Yb^{3+} , Tm^{3+} ions co-doped GdOCl nanomaterials has not been investigated.

In order to acquire a novel morphology of $\text{GdOCl}:\text{Yb}^{3+}$, Tm^{3+} nanomaterials, preparation of $\text{GdOCl}:\text{Yb}^{3+}$, Tm^{3+} nanofibers and nanobelts is an important subject to research. Up to now, no reports on the synthesis of $\text{GdOCl}:\text{Yb}^{3+}$, Tm^{3+} nanofibers and nanobelts by double-crucible method are found in the references. In particular, the morphology, structure, photoluminescence and magnetic properties of products were systematically researched. More importantly, $\text{GdOCl}:\text{Yb}^{3+}$, Tm^{3+} nanomaterials showed satisfactory luminescence properties of both UC and DC. The enhanced UC luminescence from the transitions of $^1\text{G}_4 \rightarrow ^3\text{H}_6$ and $^1\text{G}_4 \rightarrow ^3\text{F}_4$ of Tm^{3+} ions has been observed for the first time with increasing concentration of Yb^{3+} and Tm^{3+} ions, which is studied to the energy transfer from Yb^{3+} to Tm^{3+} . Furthermore, the forming mechanisms of $\text{GdOCl}:\text{Yb}^{3+}$, Tm^{3+} nanostructures are also put forward.

2 Experimental sections

2.1 Chemicals

Polyvinyl pyrrolidone (PVP, K90, $M_r = 90,000$, AR) was bought from Tiantai Chemical Co., Ltd. Gadolinium oxide (Gd_2O_3 , 99.99%), thulium oxide (Tm_2O_3 , 99.99%) and ytterbium oxide (Yb_2O_3 , 99.99%), *N,N*-dimethylformamide (DMF, AR) and ammonium chloride (NH_4Cl , AR) were purchased from Sinopharm Chemical Reagent Co., Ltd. Nitric acid (HNO_3 , AR) was bought from Beijing Chemical Works.

2.2 Preparation of $\text{GdOCl}:\text{x}\%\text{Yb}^{3+}$, $\text{y}\%\text{Tm}^{3+}$ nanofibers

Preparation of $\text{GdOCl}:\text{x}\%\text{Yb}^{3+}$, $\text{y}\%\text{Tm}^{3+}$ [$\text{y} = 0.1$ and $\text{x} = 2.5, 5, 10, 15, 20$; $\text{x} = 10$ and $\text{y} = 0.05, 0.1, 0.3, 0.5, 0.7$]; $\text{x}\%$ and $\text{y}\%$ represent molar ratio of $\text{Yb}^{3+}/(\text{Yb}^{3+} + \text{Tm}^{3+} + \text{Gd}^{3+})$ and $\text{Tm}^{3+}/(\text{Yb}^{3+} + \text{Tm}^{3+} + \text{Gd}^{3+})$, respectively nanofibers was performed by calcining and chloridizing the electrospun PVP/ $[\text{Gd}(\text{NO}_3)_3 + \text{Yb}(\text{NO}_3)_3 + \text{Tm}(\text{NO}_3)_3]$ original composite nanofibers. In the representative process of synthesizing typical $\text{GdOCl}:\text{10}\%\text{Yb}^{3+}$, $\text{0.1}\%\text{Tm}^{3+}$ nanofibers, 0.8949 g of Gd_2O_3 , 0.1082 g of Yb_2O_3 , and 0.0011 g of Tm_2O_3 were dissolved in dilute HNO_3 at high temperature, and mixed rare earth nitrates were obtained after getting rid of the water from the liquor through heated. The compounded rare earth nitrates were dissolved in 14.9626 g of DMF, after that 2.0834 g of PVP was added into the above-mentioned liquor under intensely stirring for 6 h to generate uniform lucid spinning liquid. The mass ratios of rare earth nitrates, DMF and PVP were equal to 10:79:11 in the spinning liquid. Whereafter, the spinning liquid was electrospun under the high-tension of 13 kV, and the distance between the spinneret and collector was constant at 18 cm. The ambient temperature was 20–24 °C and the relative moisture was 30–50%. The electrospun original composite nanofibers were prepared on the collector in this method. As-obtained nanofibers were calcined at 700 °C for 4 h with a heating rate of 1 °C/min in the air, then the calcining temperature was declined to 200 °C at a cooling rate of 1 °C/min, after that natural cooling down to ambient temperature, and $\text{Gd}_2\text{O}_3:\text{10}\%\text{Yb}^{3+}$, $\text{0.1}\%\text{Tm}^{3+}$ nanofibers were acquired. Using NH_4Cl powders as a chlorination source, $\text{GdOCl}:\text{10}\%\text{Yb}^{3+}$, $\text{0.1}\%\text{Tm}^{3+}$ nanofibers might be synthesized by chloridizing pre-samples. Some NH_4Cl powders were fitted into a big crucible, and carbon rods were stowed on the NH_4Cl powders, pre-samples were put on a small crucible, afterwards the small crucible was put in the big crucible, and the big crucible finally was covered with its lid. The crucibles were heated at a rate of 1 °C/min and maintained at 500 °C for 2 h, then the calcining

temperature was reduced to 200 °C at a rate of 1 °C/min, and then cooling down to ambient temperature spontaneously. The procedure is called as a double-crucible chlorination technique. Other series of $\text{GdOCl}:x\%\text{Yb}^{3+}$, $y\%\text{Tm}^{3+}$ [$x = 10$ and $y = 0.05, 0.3, 0.5, 0.7$; $y = 0.1$ and $x = 2.5, 5, 15, 20$] nanofibers were synthesized by the analogical process apart from various doping concentration of Yb^{3+} ions and Tm^{3+} ions.

2.3 Preparation of $\text{GdOCl}:10\%\text{Yb}^{3+}$, $0.1\%\text{Tm}^{3+}$ nanobelts

Gd_2O_3 (0.8949 g), Yb_2O_3 (0.1082 g) and Tm_2O_3 (0.0011 g) were dissolved in dilute HNO_3 at high temperature. The compounded rare earth nitrates were acquired by eliminating the water from the liquor. The compounded rare earth nitrates were dissolved in 13.258 g of DMF, and 3.788 g of PVP subsequently was added into the above-mentioned liquor under intensely stirring for 6 h to generate uniform lucid spinning liquid. The mass ratios of rare earth nitrates, DMF and PVP were equal to 10:70:20 in the spinning liquid. Whereafter, the spinning liquid was electrospun beneath the high-tension of 8 kV, and the distance between the spinneret and collector was constant at 15 cm, and the other fabrication criterias were identical to those for the nanofibers. The electrospun original composite nanobelts were generated on the collector by this means. $\text{GdOCl}:10\%\text{Yb}^{3+}$, $0.1\%\text{Tm}^{3+}$ nanobelts were fabricated through calcining and chloridizing of the obtained original composite nanobelts utilizing the identical process, as depicted in Sect. 2.2.

2.4 Characterization methods

X-ray diffraction (XRD) measurements were performed utilizing a Rigaku D/max-RA X-ray diffractometer with $\text{Cu K}\alpha$ radiation. The size and morphology of the products were observed by an JSM-7610F field emission scanning electron microscope (SEM). The elementary compositions of the samples were inspected by an OXFORD ISIS-300 energy dispersive spectrometer (EDS). The magnetic properties of samples were recorded by a MPMSSQUID XL magnetometer in magnetic fields up to 20 kOe. The excitation and emission spectra of products were measured with a Hitachi F-7000 fluorescence spectrophotometer equipped with a Xe lamp as the excitation source. The UC luminescence spectra were determined with Hitachi F-7000 fluorescence spectrophotometer utilizing a power-tunable 980 nm diode laser. For purpose of comparing the luminescent intensity of the products, all test conditions maintain uniform. All the measures were executed at ambient temperature.

3 Results and discussion

3.1 XRD analysis

Figure 1a reveals the XRD patterns of the obtained $\text{GdOCl}:10\%\text{Yb}^{3+}$, $y\%\text{Tm}^{3+}$ nanofibers with various Tm^{3+} concentrations from 0.05 to 0.7%. The XRD patterns agree well with the PDF standard diffraction lines (PDF#85-1199), secondary phase or impurity peaks were not discovered, revealing a single-phase tetragonal GdOCl with lattice parameters of $a = b = 3.950$, $c = 6.671$ and the space group of $P4/nmm$. The stronger diffraction peaks appear at 13.26° , 26.20° , 32.02° , 35.19° , 42.17° , 46.85° , and 59.14° correspond to the (001), (101), (102), (110), (112), (103), and (212) planes, respectively. Similar XRD patterns (Fig. 1b) for samples with different Yb^{3+} doping concentrations suggest that whole the products have been crystallized into the pure tetragonal phase. In addition, the same structures are obtained for the $\text{GdOCl}:10\%\text{Yb}^{3+}$, $0.1\%\text{Tm}^{3+}$ nanofiber and nanobelts, as manifested in Fig. 1c. The crystal structure (Fig. 1d) of GdOCl was modeled utilizing lattice parameters and atom positions. In GdOCl structure, the Gd^{3+} ion was composed of four O atoms with identical $\text{Gd}-\text{O}$ bond length and five Cl atoms having two diverse $\text{Gd}-\text{Cl}$ bond lengths. The result demonstrates that pure phase products are obtained under current synthetic condition, implying that the Yb^{3+} and Tm^{3+} ions may be doped into the GdOCl host lattice by substitution for the Gd^{3+} owing to their similar ionic radii and same valence states.

3.2 Morphology observation

The morphologies of the samples are measured by SEM. Figure 2 shows the typical SEM images of the original composite nanofibers, $\text{GdOCl}:10\%\text{Yb}^{3+}$, $0.1\%\text{Tm}^{3+}$ nanofibers, original composite nanobelts and $\text{GdOCl}:10\%\text{Yb}^{3+}$, $0.1\%\text{Tm}^{3+}$ nanobelts. From the SEM image of Fig. 2a, it can be clearly noticed that the original composite nanofibers before calcined have smooth surface and homogeneous diameter. After annealing at 700 °C and chlorinating at 500 °C, as-formed $\text{GdOCl}:10\%\text{Yb}^{3+}$, $0.1\%\text{Tm}^{3+}$ nanofibers have rough surface, as revealed in Fig. 2b. The SEM image of original composite nanobelts with a thickness of 333 nm is manifested in Fig. 2c. Clearly, uniform $\text{GdOCl}:10\%\text{Yb}^{3+}$, $0.1\%\text{Tm}^{3+}$ nanobelts with a thickness of 135 nm are prepared and possess a relatively smooth surface and the width is uniform, as shown in Fig. 2d. Under the 95% level of confidence, the diameters and widths of original composite nanofibers, nanobelts and $\text{GdOCl}:10\%\text{Yb}^{3+}$, $0.1\%\text{Tm}^{3+}$ nanofibers, nanobelts are normal distribution based on Shapiro–Wilk analytical method. Distribution histograms of diameter and width of the nanostructures are revealed in Fig. 3. It can be shown that diameters of original composite

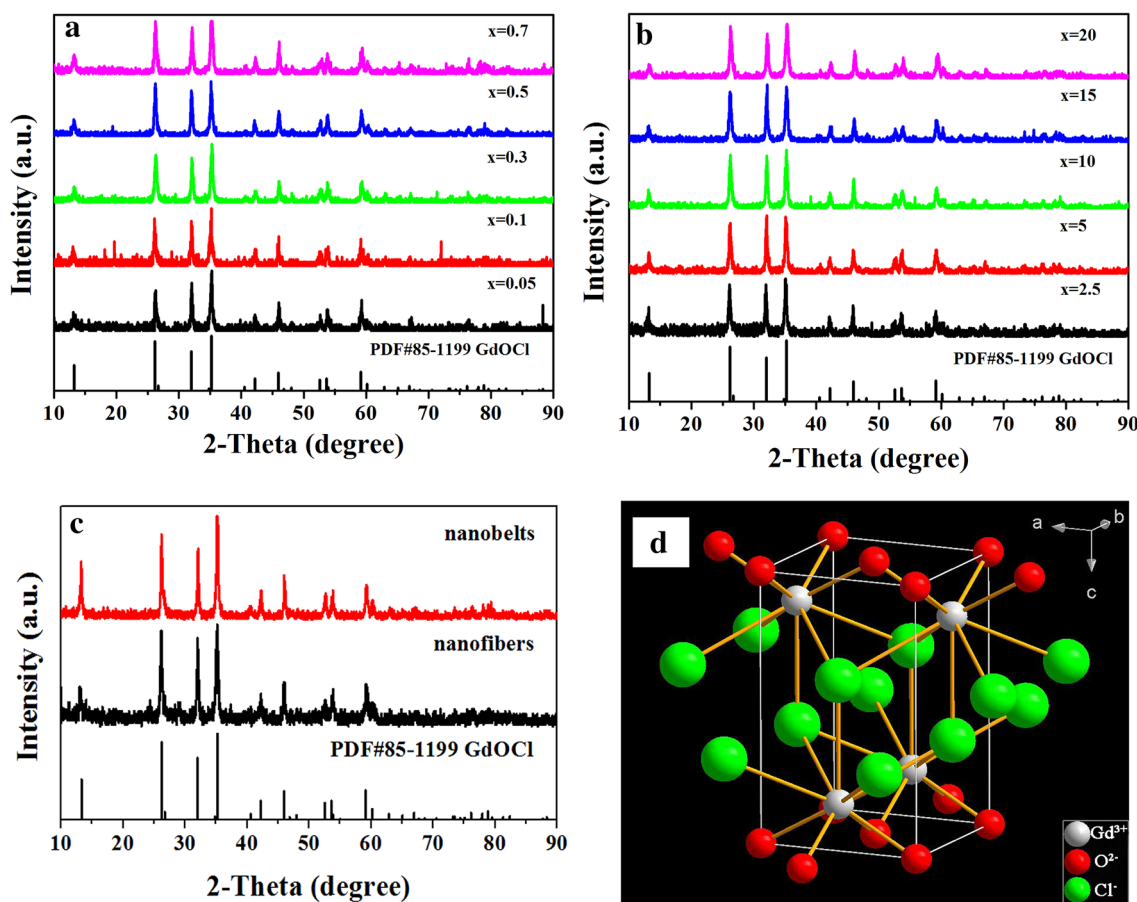


Fig. 1 XRD patterns of GdOCl:10%Yb³⁺, y%Tm³⁺ nanofibers (y=0.05, 0.1, 0.3, 0.5, and 0.7) (a), GdOCl:x%Yb³⁺, 0.1%Tm³⁺ nanofibers (x=2.5, 5, 10, 15, and 20) (b), GdOCl:10%Yb³⁺,

0.1%Tm³⁺ nanofibers and nanobelts (c) with PDF standard card of GdOCl and crystal structure of GdOCl compound (d)

nanofibers and GdOCl:10%Yb³⁺, 0.1%Tm³⁺ nanofibers are 420.25 ± 2.46 and 212.84 ± 1.04 nm, respectively and widths of original composite nanobelts and GdOCl:10%Yb³⁺, 0.1%Tm³⁺ nanobelts are 5.13 ± 0.03 and 1.07 ± 0.03 μm, respectively. After calcining at 700 °C and chloridizing at 500 °C, the diameters and widths of nanomaterials immensely reduce owing to the loss of PVP. In summary, the chlorination technique can maintain the morphologies of nanofibers and nanobelts acted as precursors.

The elementary compositions of original composite nanofibers, GdOCl:10%Yb³⁺, 0.1%Tm³⁺ nanofibers, original composite nanobelts and GdOCl:10%Yb³⁺, 0.1%Tm³⁺ nanobelts are ulteriorly verified by energy dispersive spectrometer (EDS), as presented in Fig. 4. EDS spectra reveal that C, N, O, Gd, Yb, and Tm are the primary elements in original composite nanofibers and nanobelts, and Cl, O, Yb, Tm, and Gd in GdOCl:10%Yb³⁺, 0.1%Tm³⁺ nanofibers and nanobelts. The C element in GdOCl nanomaterials is derived from conducting resin for preparing SEM measurement samples. Cu comes from copper carrier for supporting samples

and Pt is from the conductive film coated on products for SEM examination.

3.3 Photoluminescence properties

3.3.1 Up-conversion luminescence properties

The optical properties of samples are investigated as a function of the activator Tm³⁺ ions and sensitizer Yb³⁺ ions concentrations in the system. Figure 5a reveals the UC emission spectra of GdOCl:10%Yb³⁺, y%Tm³⁺ with different Tm³⁺ concentrations under 980 nm laser excitation. All the spectra show two main emission bands at 483 and 676 nm assigned to ¹G₄ → ³H₆ and ¹G₄ → ³F₄ transitions of Tm³⁺ ions, respectively. The dependence of UC luminescence emission intensity on the Tm³⁺ doped concentration of GdOCl:10%Yb³⁺, y%Tm³⁺ nanofibers is also shown in the inset of Fig. 5a. When the concentration of Yb³⁺ ions is fixed at 10%, the emission intensity of samples increases gradually with increasing in the concentration of Tm³⁺ ions. The emission

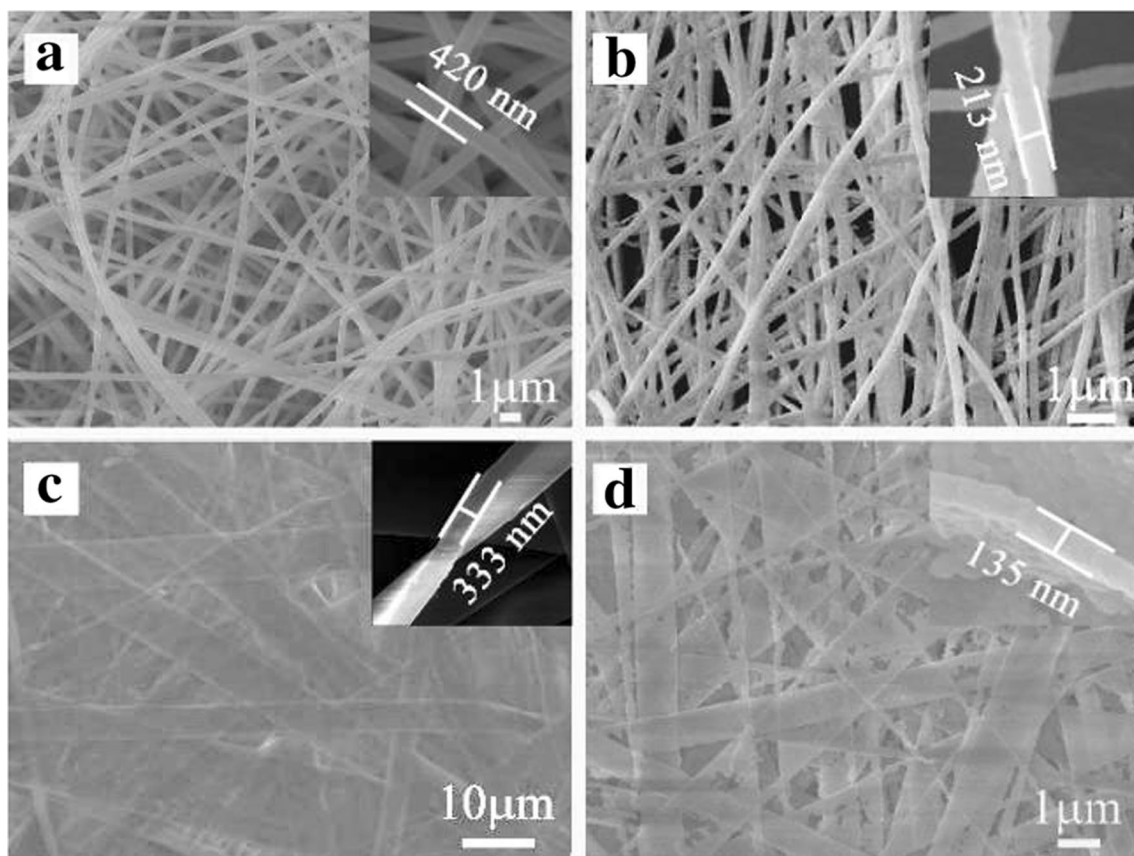


Fig. 2 SEM images of original composite nanofibers (a), GdOCl:10%Yb³⁺, 0.1% Tm³⁺ nanofibers (b), original composite nanobelts (c) and GdOCl:10%Yb³⁺, 0.1% Tm³⁺ nanobelts (d)

intensity achieves the maximum when the Tm³⁺ concentration is at 0.1%. However, as the concentration of Tm³⁺ ions further increases beyond 0.1%, an intensity decrease of UC emission is clearly seen as a result of concentration quenching effect. When the concentration of Tm³⁺ ions increase gradually, the distance between two adjacent Tm³⁺ ions or Tm³⁺ and Yb³⁺ ions decrease. As a result, the probability of cross-relaxation will be enhanced and the effective energy transfer from Yb³⁺ to Tm³⁺ will be suppressed.

Figure 5b reveals the UC emission spectra of GdOCl:x%Yb³⁺, 0.1%Tm³⁺ nanofibers. Increasing concentrations of Yb³⁺ ions for GdOCl:Yb³⁺, Tm³⁺ nanofibers, the spectral shape and location of emission peaks do not change, but the emission intensity for GdOCl:Yb³⁺, Tm³⁺ nanofibers strongly rely on the doped concentration of Yb³⁺ ions. The dependence of UC luminescence emission intensity on the Yb³⁺ doping concentration of GdOCl:x%Yb³⁺, 0.1%Tm³⁺ nanofibers is likewise shown in the inset of Fig. 5b. When the concentration of Tm³⁺ ions is immobilized at 0.1%, the emission intensity raises gradually with increasing the concentration of Yb³⁺ ions. The emission intensity attains to the maximum value when the Yb³⁺ concentration is at 10%. However, as the concentration of Yb³⁺ ions further

increases beyond 10%, an intensity decrease of UC emission is clearly seen as a result of concentration quenching effect. When the doping ratio between Yb³⁺ and Tm³⁺ is 10:0.1 for GdOCl:Yb³⁺, Tm³⁺ nanofibers, the strongest emission spectra can be acquired.

Excited by a 980 nm diode laser with different pump powers, emission spectra of GdOCl:10%Yb³⁺, 0.1%Tm³⁺ nanofibers are gained, as presented in Fig. 6a. It is clearly shown that the UC luminescence intensity of GdOCl:10%Yb³⁺, 0.1%Tm³⁺ nanofibers raises with the increase of pump powers. The UC emission intensity increased with power obeying a rule $I \propto P^n$ for blue emission, where I is the UC emission intensity, P is the excitation laser power, and n is the number of photons [45]. Figure 6b shows the natural logarithm plots of the emission intensity as a function of pump power for the blue (483 nm) emission in GdOCl:10%Yb³⁺, 0.1%Tm³⁺ nanofibers. It may be judged that photon avalanche mechanism of the nanofibers is eliminated due to inexistence of sharp change. For the emission, the value of n (the slope) in GdOCl:10%Yb³⁺, 0.1%Tm³⁺ is determined to be 2.54. Generally speaking, a straight line with the slope ~ 3 for the UC luminescence manifests that three photons are drawn into this UC luminescence

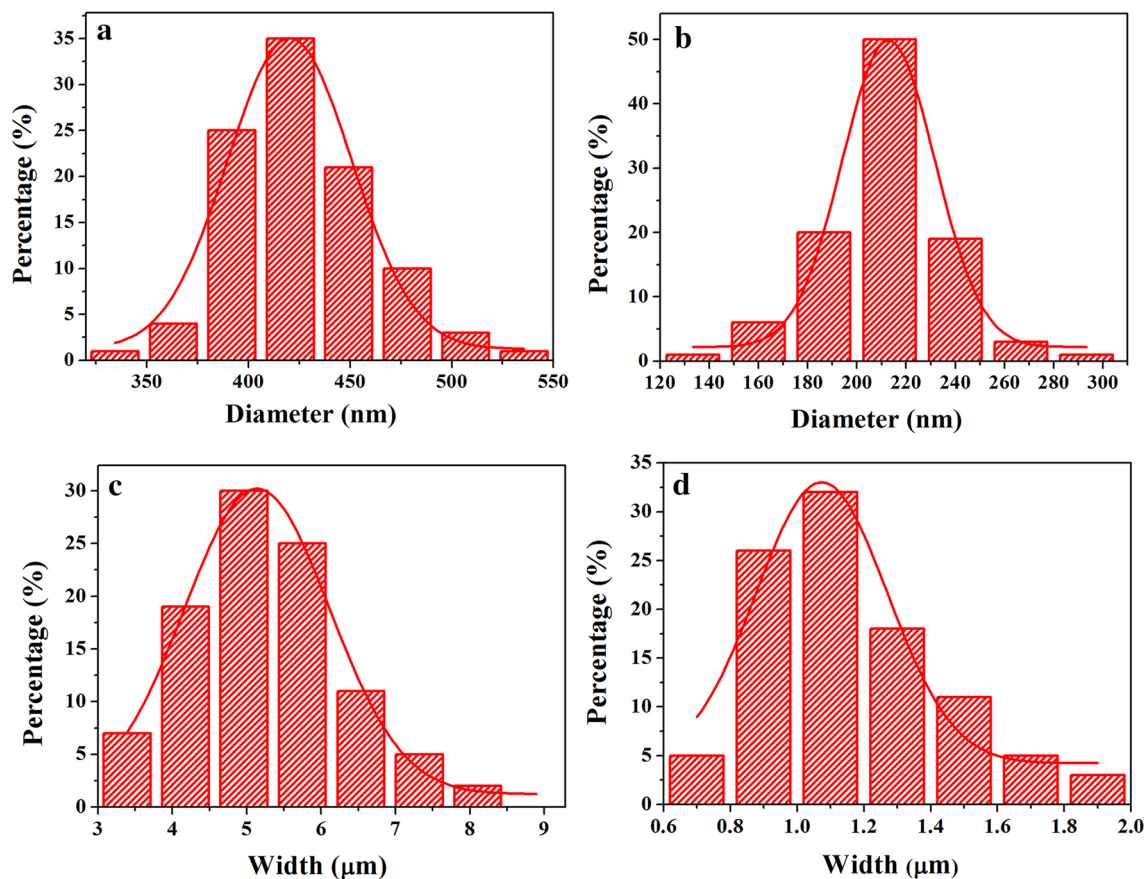


Fig. 3 Distribution histograms of the diameters of original composite nanofibers (a), GdOCl:10%Yb³⁺, 0.1%Tm³⁺ nanofibers (b) and widths of original composite nanobelts (c), GdOCl:10%Yb³⁺, 0.1%Tm³⁺ nanobelts (d)

procedure. It is testified from the aforementioned research that the blue emission of GdOCl:10%Yb³⁺, 0.1%Tm³⁺ is three photons process.

Figure 7 demonstrates the comparison of the UC emission spectra between the GdOCl:10%Yb³⁺, 0.1%Tm³⁺ nanofibers and nanobelts beneath the same measured conditions. It can be discovered that the nanobelts have higher luminescent intensity than nanofibers. It is generally known that the specific surface area of the nanobelts is smaller than that of the nanofibers, suggesting that the nanobelts have less surface defect than the nanofibers [46, 47]. As a consequence, the nanobelts have stronger luminescence intensity than the nanofibers.

Generally speaking, color is stood for by the Commission Internationale de L'Eclairage (CIE) chromaticity coordinates. For the GdOCl:10%Yb³⁺, y%Tm³⁺ nanofibers, the chromaticity coordinates (X, Y) are ensured to be [(0.101, 0.151), (0.100, 0.133), (0.098, 0.134), (0.074, 0.237) and (0.064, 0.281)], which correspond to the Tm³⁺ concentration of 0.05, 0.1, 0.3, 0.5 and 0.7%, respectively. Apparently, the emission color of GdOCl:10%Yb³⁺, y%Tm³⁺ nanofibers shifts from blue to blueish green along with the change

of concentrations of Tm³⁺ ions, as presented in Fig. 8a. Analogously, CIE chromaticity coordinates diagram for GdOCl:x%Yb³⁺, 0.1%Tm³⁺ nanofibers is shown in Fig. 8b. The chromaticity coordinates (X, Y) are [(0.098, 0.133), (0.098, 0.134), (0.100, 0.133), (0.090, 0.165) and (0.080, 0.209)], which correspond to the Yb³⁺ concentration of 2.5, 5, 10, 15 and 20%, respectively. The emission color of GdOCl:x%Yb³⁺, 0.1%Tm³⁺ (x = 2.5, 5, 10, 15 and 20) nanofibers is regulated from blue to greenish blue. The CIE chromaticity coordinates of GdOCl:10%Yb³⁺, 0.1%Tm³⁺ nanofibers (0.098, 0.134) and nanobelts (0.103, 0.124) are represented in Fig. 8c. The results manifest that the emitting color may be adjusted by varying the doping concentration of ions and the morphologies of nanostructures.

3.3.2 Down-conversion luminescence properties

In order to research the effects of Yb³⁺ and Tm³⁺ doped concentration on down-conversion luminescence properties, we research the photoluminescence excitation and emission spectra of a series of GdOCl:10%Yb³⁺, y%Tm³⁺ (y = 0.05, 0.1, 0.3, 0.5 and 0.7) and GdOCl:x%Yb³⁺, 0.1%Tm³⁺

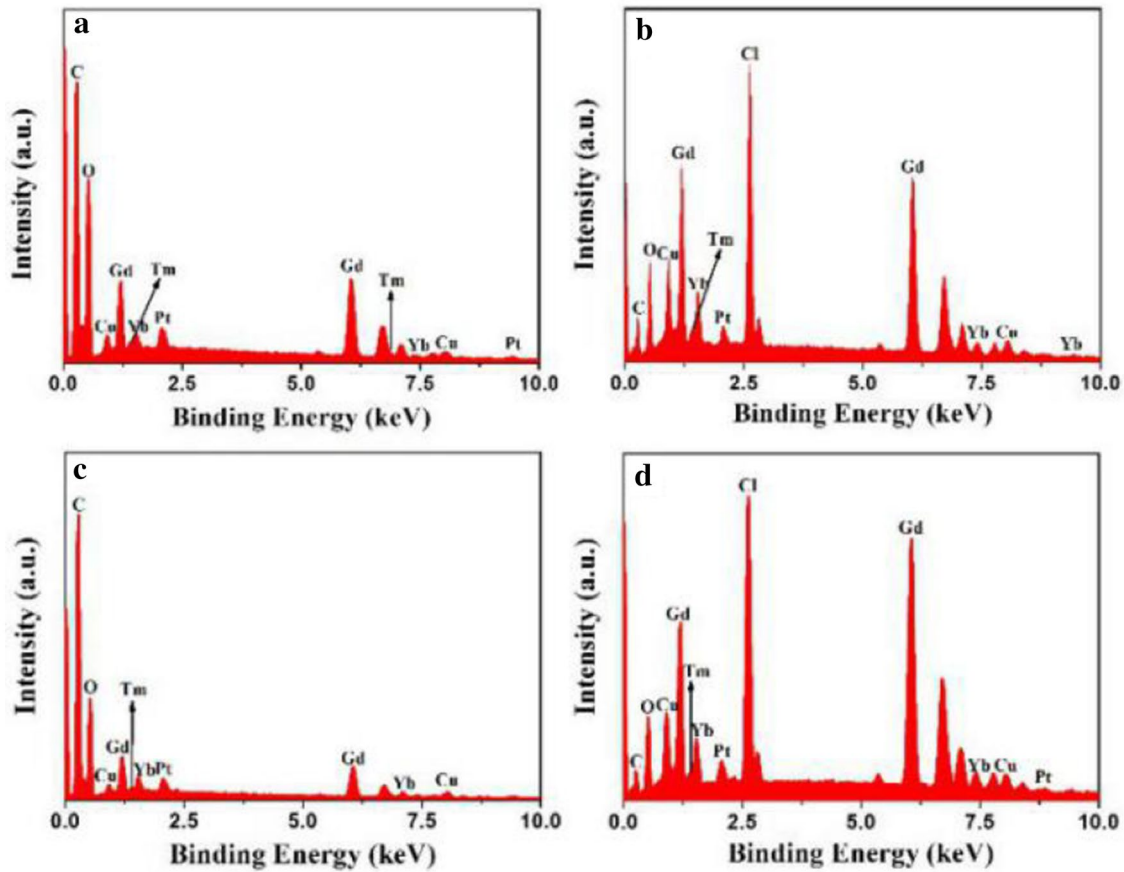


Fig. 4 EDS spectra of original composite nanofibers (a), GdOCl:10%Yb³⁺, 0.1% Tm³⁺ nanofibers (b), original composite nanobelts (c) and GdOCl:10%Yb³⁺, 0.1% Tm³⁺ nanobelts (d)

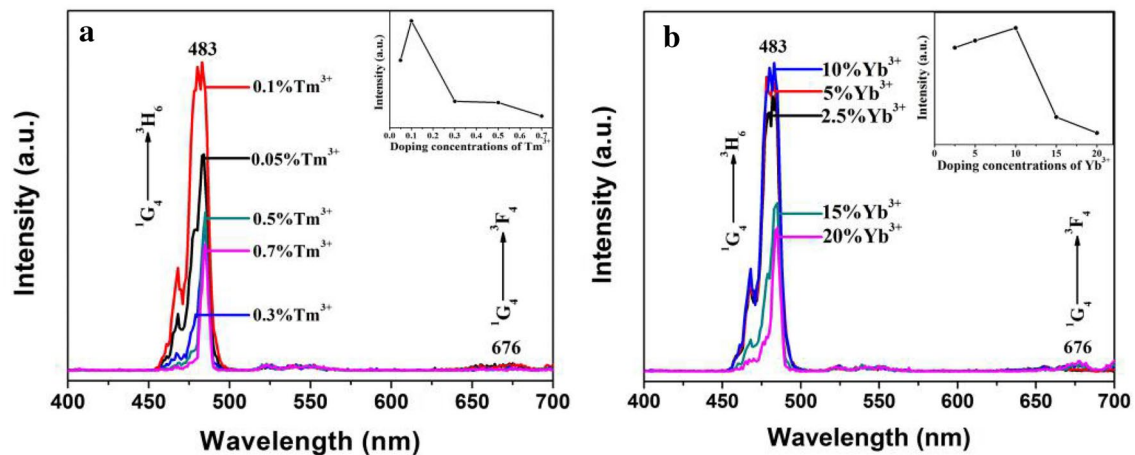


Fig. 5 UC emission spectra of GdOCl:10%Yb³⁺, y%Tm³⁺ nanofibers (y=0.05, 0.1, 0.3, 0.5 and 0.7) (a) and GdOCl:x%Yb³⁺, 0.1%Tm³⁺ nanofibers (x=2.5, 5, 10, 15 and 20) (b) excited by 980 nm diode laser with the pump power of 1393 mW. The inset are the dependence

of its PL intensity on the Tm³⁺ content in GdOCl:Yb³⁺, Tm³⁺ nanofibers (a) and the Yb³⁺ content in GdOCl:Yb³⁺, Tm³⁺ nanofibers (b)

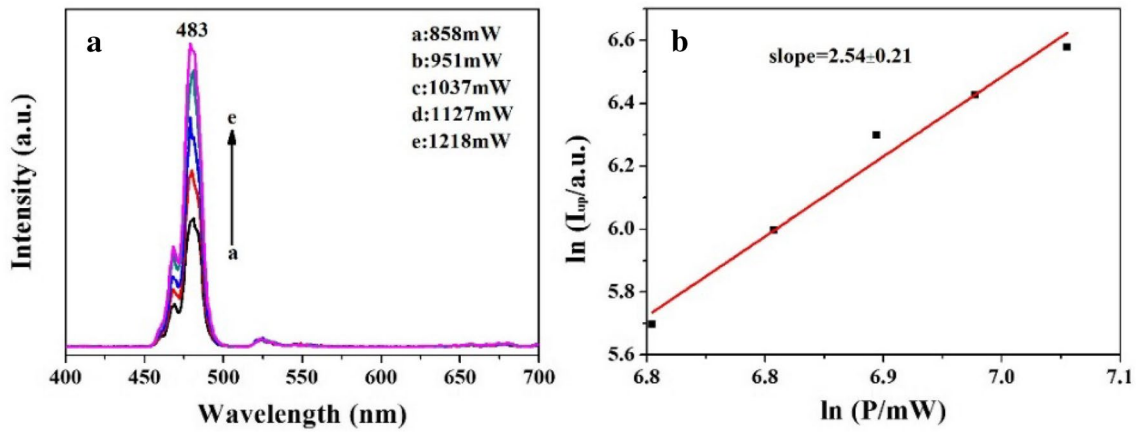


Fig. 6 UC emission spectra of GdOCl:10%Yb³⁺, 0.1%Tm³⁺ nanofibers excited by a 980 nm diode laser at various pump power (a) and plots of natural logarithm up-conversion emission intensity (I_{up}) versus natural logarithm pump power of diode laser (P) for GdOCl:10%Yb³⁺, 0.1%Tm³⁺ nanofibers (b)

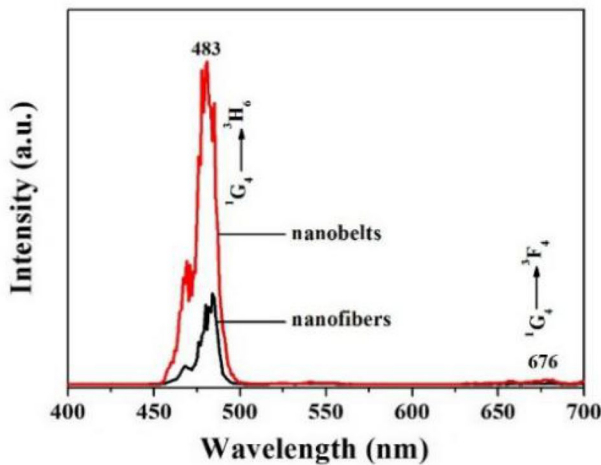


Fig. 7 UC emission spectra of GdOCl:10%Yb³⁺, 0.1%Tm³⁺ nanofibers (black line) and nanobelts (red line) excited by 980 nm diode laser with the pump power of 1393 mW. (Color figure online)

($x=2.5, 5, 10, 15$ and 20) nanofibers, as demonstrated in Figs. 9 and 10. The excitation spectra (Figs. 9a, 10a) of GdOCl:10%Yb³⁺, $y\%$ Tm³⁺ ($y=0.05, 0.1, 0.3, 0.5$ and 0.7) and GdOCl: $x\%$ Yb³⁺, 0.1%Tm³⁺ ($x=2.5, 5, 10, 15$ and 20) nanofibers consist of a strong absorption band attributed to the transition of ³H₆ → ¹D₂ of Tm³⁺ at 357 nm. Upon the 357-nm excitation, the emission spectra of the as-obtained GdOCl:10%Yb³⁺, $y\%$ Tm³⁺ ($y=0.05, 0.1, 0.3, 0.5$ and 0.7) (Fig. 9b) and GdOCl: $x\%$ Yb³⁺, 0.1%Tm³⁺ ($x=2.5, 5, 10, 15$ and 20) nanofibers (Fig. 10b) exhibit blue emissions due to ¹D₂ → ³F₄ (Tm³⁺, 458 nm) transition. With the increase of Tm³⁺ concentrations, blue emission band at 458 nm (¹D₂ → ³F₄) of Tm³⁺ increases until a maximum intensity is reached at the Tm³⁺ concentration of around

0.5%, and then reduces owing to concentration quenching effect, which is attributed to the cross relaxation between adjacent Tm³⁺ ions. When we fixed the doped concentration of Tm³⁺ ions as 0.1%, the emission intensities of Tm³⁺ decrease with increasing in Yb³⁺ concentrations as shown in Fig. 10b, which strongly suggests the cross relaxation from Tm³⁺ to Yb³⁺, attributed to ³H₄ (Tm³⁺) + ²F_{7/2} (Yb³⁺) → ³H₆ (Tm³⁺) + ²F_{5/2} (Yb³⁺). The results also have been confirmed by other researchers [48]. The CIE chromaticity coordinates of GdOCl:10%Yb³⁺, $y\%$ Tm³⁺ and GdOCl: $x\%$ Yb³⁺, 0.1%Tm³⁺ nanofibers are shown in Fig. 11. Under UV irradiation (357 nm), GdOCl doped with Yb³⁺ and Tm³⁺ nanofibers show blue light. Chromaticity coordinates of GdOCl:Yb³⁺, Tm³⁺ nanofibers are listed in Table 1.

3.4 Energy transfer mechanism

In principle, there exist four basic mechanisms of population included in the UC process, i.e., ground state absorption (GSA), excited state absorption (ESA), energy transfer (ET), and photon avalanche (PA). For the UC luminescence mechanisms of GdOCl:Yb³⁺, Tm³⁺ nanofibers, PA can be excluded directly because there is no obvious turning point in the energy. The three photons process in GdOCl:Yb³⁺, Tm³⁺ nanofibers may occur sequentially through GSA, ESA, and ET processes. Figure 12 reveals the probable UC mechanism of Yb³⁺ ions and Tm³⁺ ions. Under excitation at 980 nm, the Yb³⁺ ions consecutively absorb 980 nm photons, and then transfer the energies to the ³H₅, ³F₂, and ¹G₄ levels in the Tm³⁺ ion. Subsequently, radiationless multi-phonon decay of ³H₅ → ³F₄ also inhabits the ³F₄ level and nonradiative relaxation leads to population of the ³H₄ level from ³F₂ level. Finally, the blue emission centered at 483 nm (Tm³⁺, ¹G₄ → ³H₆) and the quite weak

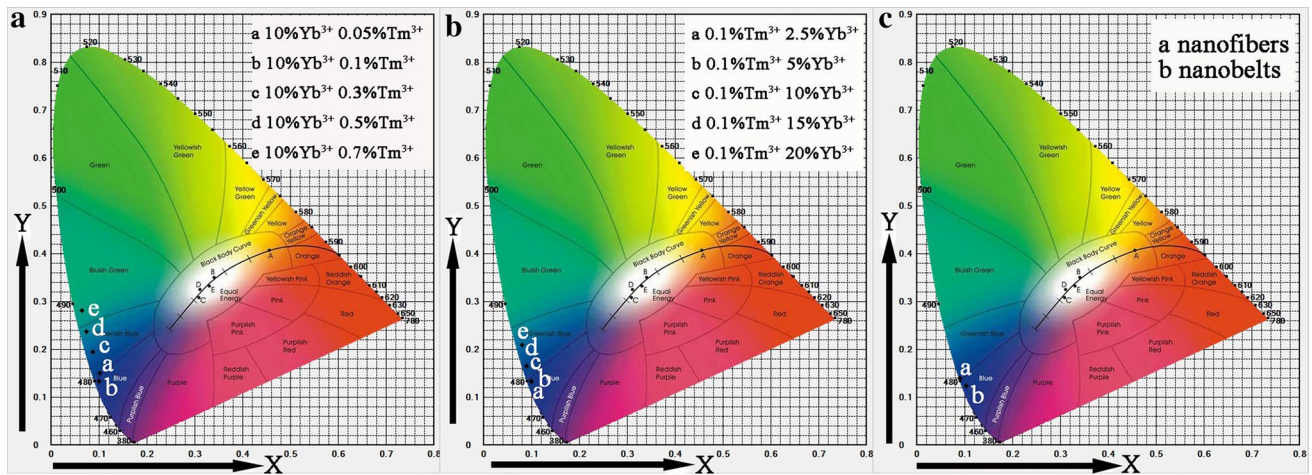


Fig. 8 CIE chromaticity coordinates diagrams of GdOCl:10%Yb³⁺, y%Tm³⁺ (y=0.05, 0.1, 0.3, 0.5 and 0.7) nanofibers (a), GdOCl:x%Yb³⁺, 0.1%Tm³⁺ (x=2.5, 5, 10, 15 and 20) nanofibers (b) and GdOCl:10%Yb³⁺, 0.1%Tm³⁺ nanostructures (c)

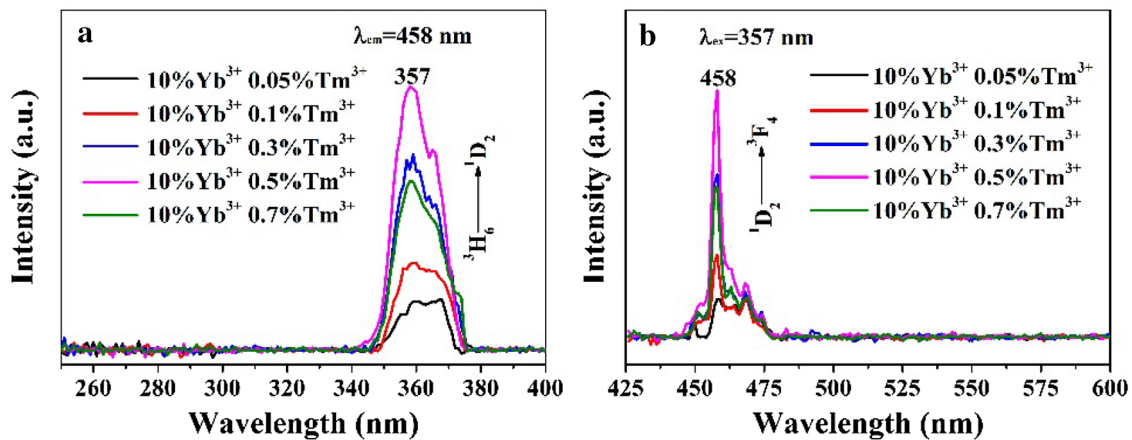


Fig. 9 Excitation (a) and emission (b) spectra of GdOCl:10%Yb³⁺, y%Tm³⁺ nanofibers

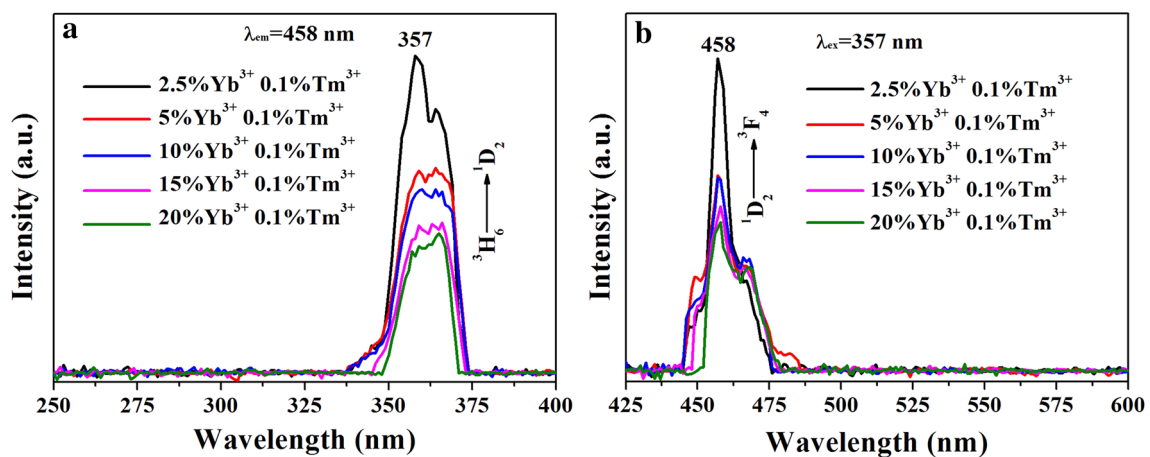


Fig. 10 Excitation (a) and emission (b) spectra of GdOCl:x%Yb³⁺, 0.1%Tm³⁺ nanofibers

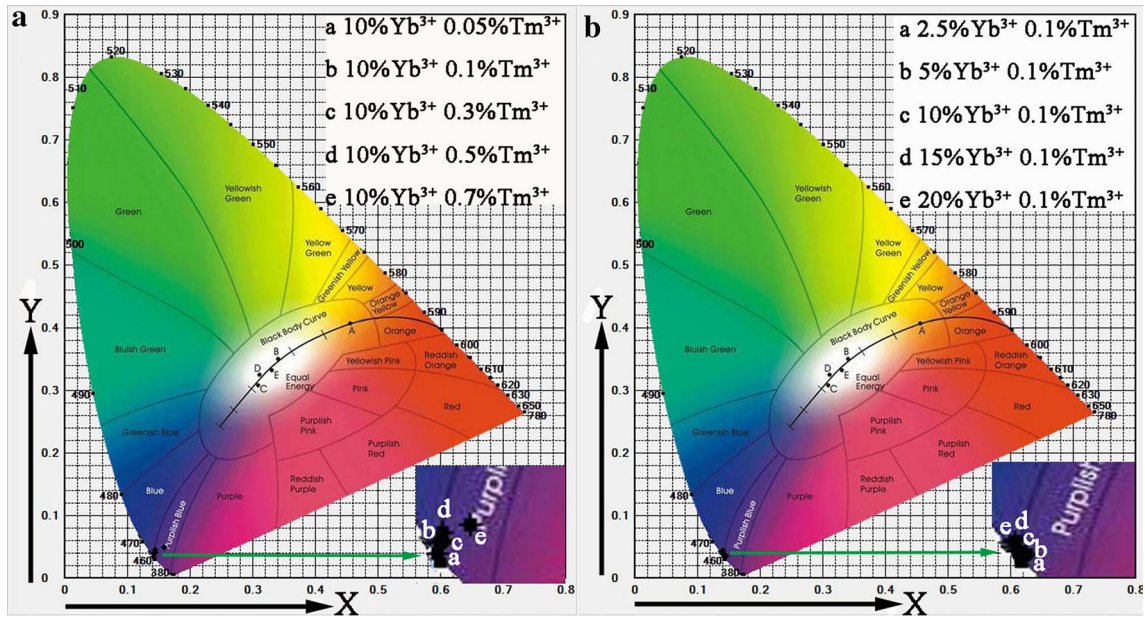


Fig. 11 CIE chromaticity coordinates diagrams of GdOCl:10%Yb³⁺, y%Tm³⁺ (y=0.05, 0.1, 0.3, 0.5 and 0.7) (a) and GdOCl:x%Yb³⁺, 0.1%Tm³⁺ (x=2.5, 5, 10, 15 and 20) nanofibers (b)

Table 1 Chromaticity coordinates of GdOCl:Yb³⁺, Tm³⁺ nanofibers

Samples	Chromaticity coordinate	Samples	Chromaticity coordinate
GdOCl:10%Yb ³⁺ , 0.05%Tm ³⁺	(0.141, 0.035)	GdOCl:2.5%Yb ³⁺ , 0.1%Tm ³⁺	(0.146, 0.036)
GdOCl:10%Yb ³⁺ , 0.1%Tm ³⁺	(0.143, 0.040)	GdOCl:5%Yb ³⁺ , 0.1%Tm ³⁺	(0.144, 0.034)
GdOCl:10%Yb ³⁺ , 0.3%Tm ³⁺	(0.144, 0.042)	GdOCl:10%Yb ³⁺ , 0.1%Tm ³⁺	(0.143, 0.033)
GdOCl:10%Yb ³⁺ , 0.5%Tm ³⁺	(0.144, 0.045)	GdOCl:15%Yb ³⁺ , 0.1%Tm ³⁺	(0.142, 0.037)
GdOCl:10%Yb ³⁺ , 0.7%Tm ³⁺	(0.159, 0.049)	GdOCl:20%Yb ³⁺ , 0.1%Tm ³⁺	(0.140, 0.044)

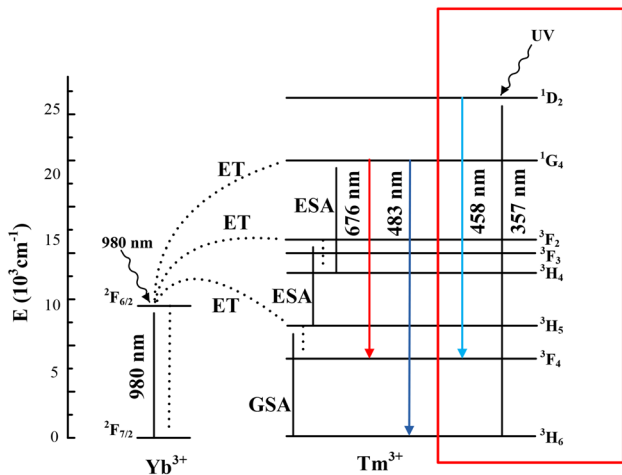


Fig. 12 Schematic energy level diagram of Yb³⁺ and Tm³⁺ in GdOCl

red emissions at 676 nm (Tm³⁺, ¹G₄ → ³F₄) is then emitted. In the DC process (red frame), under excitation at 357-nm (Tm³⁺, ³H₆ → ¹D₂) light, blue emission is achieved due to ¹D₂ → ³F₄ (Tm³⁺, 458 nm) transition.

3.5 Magnetic properties

The magnetic properties of GdOCl:x%Yb³⁺, y%Tm³⁺ (x = 10, y = 0.05, 0.1, 0.3, 0.5, 0.7; and y = 0.1, x = 2.5, 5, 10, 15, 20) nanofibers were measured by a MPMSS-QUID XL magnetometer in magnetic fields up to 20 kOe. GdOCl:x%Yb³⁺, y%Tm³⁺ samples present nice paramagnetic properties, as shown in Fig. 13. The magnetization value of GdOCl:10%Yb³⁺, 0.1%Tm³⁺ samples is 2.33 emu g⁻¹ at 20 kOe. The dependence of magnetization on the Tm³⁺ doping concentration of GdOCl:10%Yb³⁺, y%Tm³⁺ nanofibers is also shown in Fig. 13a. When the concentration of Yb³⁺ ions is immobilized at 10%, magnetizations decrease gradually with increasing the concentration of Tm³⁺ ions. The dependence of magnetizations on the Yb³⁺ doped

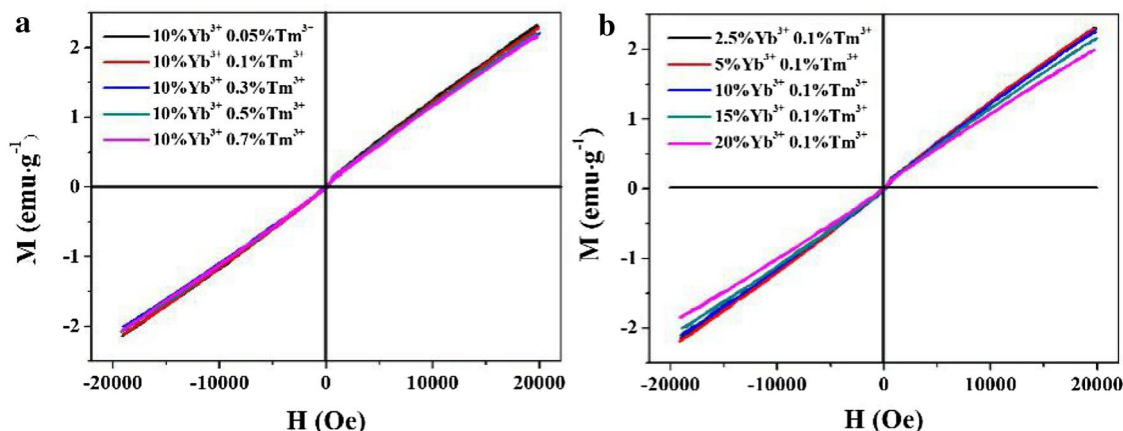


Fig. 13 Room-temperature magnetization curves of GdOCl:10%Yb³⁺, y%Tm³⁺ (y=0.05, 0.1, 0.3, 0.5 and 0.7) nanofibers (a) and GdOCl:x%Yb³⁺, 0.1%Tm³⁺ (x=2.5, 5, 10, 15 and 20) nanofibers (b)

concentration of GdOCl:x%Yb³⁺, 0.1%Tm³⁺ nanofibers is also shown in Fig. 13b. When the concentration of Tm³⁺ ions is immobilized at 0.1%, magnetizations decrease gradually with increasing the concentration of Yb³⁺ ions, because magnetic moments of Yb³⁺ and Tm³⁺ ions are smaller than that of Gd³⁺ ions. The magnetizations of products are listed in Table 2. The results indicate their underlying applications in the realms of clinical medicine and biological labeling.

3.6 Formation mechanism for the GdOCl:Yb³⁺, Tm³⁺ nanomaterials

Formation mechanism of GdOCl:Yb³⁺, Tm³⁺ nanostructures is presented in Fig. 14. PVP, Gd(NO₃)₃, Yb(NO₃)₃ and Tm(NO₃)₃ were dissolved with DMF to generate precursor liquor. Gd³⁺, Yb³⁺, Tm³⁺, and NO₃⁻ were mixed or assimilated onto PVP to form sol possessing definite viscosity. Afterwards, original composite nanofibers and nanobelts were prepared via electrospinning. PVP is template in the generation of Gd₂O₃:Yb³⁺, Tm³⁺ nanofibers and nanobelts. In the procedure

of heating, PVP was oxidized to destroy the branched chain and then to evaporate. Nitrates occur decomposition and oxidation reaction to generate NO₂, and Gd³⁺, Yb³⁺, Tm³⁺ was oxidized to produce Gd₂O₃:Yb³⁺, Tm³⁺ crystallites that were merged into nanofibers and nanobelts. Gd₂O₃:Yb³⁺, Tm³⁺ nanofibers and nanobelts were chlorinated utilizing NH₄Cl served as chlorinated source. The double-crucible technology played a vital effect in the chlorination course. First of all, NH₄Cl decomposed and reacted with Gd₂O₃:Yb³⁺, Tm³⁺ nanofibers and nanobelts to produce generate (NH₄)₃GdCl₆:Yb³⁺, Tm³⁺ nanostructures in the chlorination course. NH₄Cl powders and Gd₂O₃:Yb³⁺, Tm³⁺ nanofibers and nanobelts were isolated by carbon rods which available avoided Gd₂O₃:Yb³⁺, Tm³⁺ nanofibers and nanobelts from breaking morphology in the process. Carbon rods played a remarkable reduction effect via incorporation with O₂ to generate CO, which reacted with the oxide of Gd₂O₃:Yb³⁺, Tm³⁺ to give CO₂ in the heating procedure. (NH₄)₃GdCl₆:Yb³⁺, Tm³⁺ resolved to ammonia, hydrogen chloride and GdOCl:Yb³⁺, Tm³⁺ [49]. Reaction schemes for production of GdOCl:Yb³⁺, Tm³⁺ nanofibers and nanobelts proceed as follows:

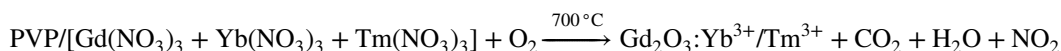
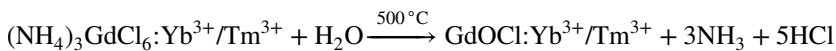
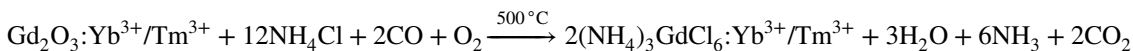
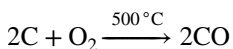
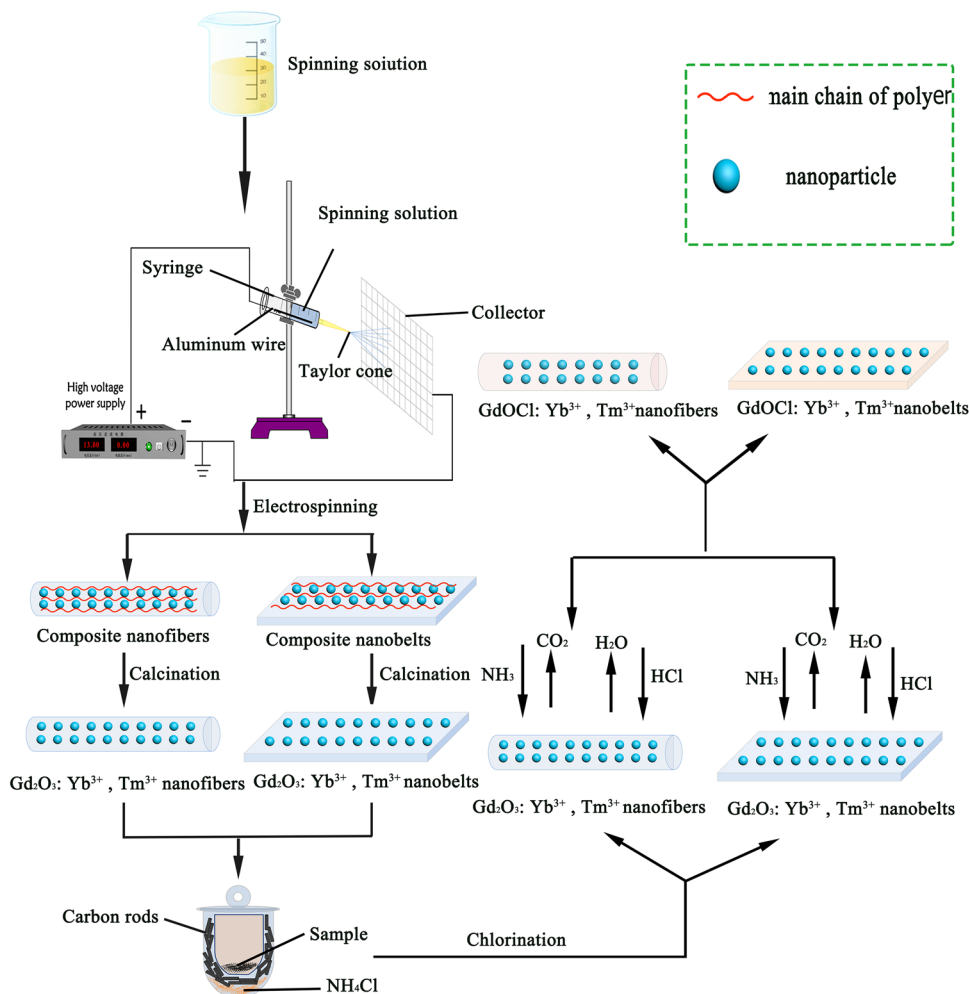


Table 2 Magnetization (M) of GdOCl:Yb³⁺, Tm³⁺ nanofibers

Samples	M (emu g ⁻¹)	Samples	M (emu g ⁻¹)
GdOCl:10%Yb ³⁺ , 0.05%Tm ³⁺	2.33	GdOCl:2.5%Yb ³⁺ , 0.1%Tm ³⁺	2.31
GdOCl:10%Yb ³⁺ , 0.1%Tm ³⁺	2.28	GdOCl:5%Yb ³⁺ , 0.1%Tm ³⁺	2.30
GdOCl:10%Yb ³⁺ , 0.3%Tm ³⁺	2.21	GdOCl:10%Yb ³⁺ , 0.1%Tm ³⁺	2.28
GdOCl:10%Yb ³⁺ , 0.5%Tm ³⁺	2.20	GdOCl:15%Yb ³⁺ , 0.1%Tm ³⁺	2.16
GdOCl:10%Yb ³⁺ , 0.7%Tm ³⁺	2.18	GdOCl:20%Yb ³⁺ , 0.1%Tm ³⁺	1.99

Fig. 14 Schematic diagram of formation mechanism of GdOCl:Yb³⁺, Tm³⁺ nanofibers and nanobelts



nanostructures exhibit bright blue emission in the nearby of 450–500 nm due to the contribution of the ¹G₄ → ³H₆ transitions of Tm³⁺ ions. The relative intensity of blue

4 Conclusions

The pure tetragonal-phase GdOCl:Yb³⁺, Tm³⁺ one-dimensional nanofibers and nanobelts have been resoundingly synthesized by electrospinning technique coupled with a double-crucible chlorination method. The diameter and width of the GdOCl:Yb³⁺, Tm³⁺ nanofibers and nanobelts are 212.84 ± 1.04 nm and 1.07 ± 0.03 μm, respectively. Beneath the excitation of 357-nm ultraviolet and 980-nm near-infrared light, Yb³⁺ and Tm³⁺ ions co-doped GdOCl

luminescence is changed after adjusting the doping concentration ratio of Yb³⁺ ion and Tm³⁺ ion. The blue emission of GdOCl:10%Yb³⁺, 0.1%Tm³⁺ nanostructures is three-photon process in the up-conversion luminescence process. Moreover, the as-prepared nanomaterials not only possess dual-mode (DC and UC) luminescence, but also exhibit paramagnetic properties at ambient temperature. The results suggest that the as-fabricated samples can be a potential and hopeful material for biological medicine, luminous lighting.

Acknowledgements This work was financially supported by National Natural Science Foundation of China (Grant Nos. 51573023, 50972020), Natural Science Foundation of Jilin Province of China (20170101101JC), Industrial Technology Research and Development Project of Jilin Province Development and Reform Commission (2017C051), Science and Technology Research Planning Project of the Education Department of Jilin Province during the 13th five-year plan period (JJKH20170608KJ), and Youth Foundation of Changchun University of Science and Technology (No. XQNJJ-2016-01).

References

- R. Saraf, C. Shivakumara, N. Dhananjaya, S. Behera, H. Nagabhushana, *J. Mater. Sci.* **50**, 287–298 (2015)
- H. Li, G. Liu, J. Wang, X. Dong, W. Yu, *New J. Chem.* **41**, 1609–1617 (2017)
- P.F.S. Pereira, I.C. Nogueira, E. Longo, E.J. Nassar, I.L.V. Rosa, L.S. Cavalcante, *J. Rare Earth* **33**, 113–128 (2015)
- H. Wang, D. Tu, J. Xu, X. Shang, P. Hu, R. Li, W. Zheng, Z. Chen, X. Chen, *J. Mater. Chem. B* **5**, 4827–4834 (2017)
- H.-S. Cho, Z. Dong, G.M. Pauletti, J. Zhang, H. Xu, H. Gu, L. Wang, R.C. Ewing, C. Huth, F. Wang, D. Shi, *ACS Nano* **4**, 5398–5404 (2010)
- Y. Chou, C. Shao, X. Li, C. Su, H. Xu, M. Zhang, P. Zhang, X. Zhang, Y. Liu, *Appl. Surf. Sci.* **285**, 509–516 (2013)
- M. Zhang, C. Shao, P. Zhang, C. Su, X. Zhang, P. Liang, Y. Sun, Y. Liu, *J. Hazard. Mater.* **225**, 155–163 (2012)
- D. Liu, Z. Wang, *Polymer* **49**, 4960–4967 (2008)
- K.R. Kort, S. Banerjee, *J. Phys. Chem. B* **117**, 1585–1591 (2013)
- G.R. Waetzig, G.A. Horrocks, J.W. Jude, L. Zuin, S. Banerjee, *Nanoscale* **8**, 979–986 (2016)
- J. Wang, H. Huang, D. Zhang, M. Chen, Y. Zhang, X. Yu, L. Zhou, Q. Wang, *Nano Res.* **8**, 2548–2561 (2015)
- Z. Chen, L. Zhang, Y. Sun, J. Hu, D. Wang, *Adv. Funct. Mater.* **19**, 3815–3820 (2009)
- S. Gai, C. Li, P. Yang, J. Lin, *Chem. Rev.* **114**, 2343–2389 (2014)
- T. Konishi, M. Shimizu, Y. Kameyama, K. Soga, *J. Mater. Sci.* **18**, 183–186 (2007)
- G. Li, J. Lin, *Chem. Soc. Rev.* **43**, 7099–7131 (2014)
- Z. Huang, H. Zhang, S. Zhang, *CrystEngComm* **19**, 2971–2976 (2017)
- J. Lee, Q. Zhang, F. Saito, *J. Solid State Chem.* **160**, 469–473 (2001)
- X. Huang, B. Li, H. Guo, *J. Alloys Compd.* **695**, 2773–2780 (2017)
- R. Yang, G. Qin, D. Zhao, K. Zheng, W. Qin, *J. Fluorine Chem.* **140**, 38–42 (2012)
- Y. Yang, C. Zhang, Y. Xu, H. Wang, X. Li, C. Wang, *Mater. Lett.* **64**, 147–150 (2010)
- B. Dong, Z. Li, Z. Li, X. Xu, M. Song, W. Zheng, C. Wang, S.S. Al-Deyab, M. El-Newehy, *J. Am. Ceram. Soc.* **93**, 3587–3590 (2010)
- D. Li, Q.L. Ma, Y. Song, X. Xi, X.T. Dong, W.S. Yu, J.X. Wang, G.X. Liu, *RSC Adv.* **6**, 113045–113052 (2016)
- S. Wei, M. Zhou, W. Du, *Sens. Actuators B* **160**, 753–759 (2011)
- X.T. Dong, L. Li, J.X. Wang, G.X. Liu, *Chem. J. Chin. Univ.* **31**, 20–25 (2010)
- C.X. Zheng, D. Li, Q.L. Ma, Y. Song, X.T. Dong, X.L. Wang, W.S. Yu, J.X. Wang, G.X. Liu, *Chem. Eng. J.* **310**, 91–101 (2017)
- Y. Liu, X. Yan, J. Lan, Y. Yu, X. Yang, Y. Lin, *Mater. Chem. Front.* **1**, 1331–1337 (2017)
- Q.L. Ma, J.X. Wang, X.T. Dong, W.S. Yu, G.X. Liu, J. Xu, *J. Mater. Chem.* **22**, 14438–14442 (2012)
- Y. Liu, J.X. Wang, X.T. Dong, G.X. Liu, *Chem. J. Chin. Univ.* **31**, 1291–1296 (2010)
- P. Kumar, B.K. Gupta, *RSC Adv.* **5**, 24729–24736 (2015)
- B.K. Gupta, T.N. Narayanan, S.A. Vithayathil, Y. Lee, S. Koshy, A.L.M. Reddy, A. Saha, V. Shanker, V.N. Singh, B.A. Kaipparattu, *Small* **8**, 3028–3034 (2012)
- P. Kumar, J. Dwivedi, B. Gupta, *J. Mater. Chem. C* **2**, 10468–10475 (2014)
- J. Dwivedi, P. Kumar, A. Kumar, Sudama, V.N. Singh, B.P. Singh, S.K. Dhawan, V. Shankera, B.K. Gupta, *RSC Adv.* **4**, 54936–54947 (2014)
- J. Xu, M. Sun, Y. Kuang, H. Bi, B. Liu, D. Yang, R. Lv, S. Gai, F. He, P. Yang, *Dalton Trans.* **46**, 1495 (2017)
- X. Huang, *J. Alloys Compd.* **690**, 356–359 (2017)
- X. Huang, *Opt. Lett.* **40**, 5231–5234 (2015)
- R.S. Yadav, R.V. Yadav, A. Bahadur, S.B. Rai, *RSC Adv.* **6**, 51768–51776 (2016)
- D. Kasprovicz, P. Gluchowski, M.G. Brik, M.M. Makowski, M. Chrunik, A. Majchrowski, *J. Alloys Compd.* **684**, 271–281 (2016)
- Q. Zhao, B. Shao, W. Lü, W. Lv, M. Jiao, L. Zhao, H. You, *Dalton Trans.* **44**, 3745–3752 (2015)
- D. Li, W. Qin, T. Aidilibike, P. Zhang, S. Liu, L. Wang, S. Li, *J. Alloys Compd.* **675**, 31–36 (2016)
- D. Li, Q.L. Ma, X. Xi, X.T. Dong, W.S. Yu, J.X. Wang, G.X. Liu, *Chem. Eng. J.* **309**, 230–239 (2017)
- Z.L. Wang, J.H. Hao, H.L.W. Chan, *J. Mater. Chem.* **20**, 3178–3185 (2010)
- X. Huang, *Dyes Pigm.* **130**, 99–105 (2016)
- X. Huang, *J. Alloys Compd.* **628**, 240–244 (2015)
- H. Li, G. Liu, J. Wang, X. Dong, W. Yu, *Phys. Chem. Chem. Phys.* **18**, 21518 (2016)
- L. Tu, X. Liu, F. Wu, H. Zhang, *Chem. Soc. Rev.* **44**, 1331 (2015)
- Q.L. Kong, J.X. Wang, X.T. Dong, W.S. Yu, G.X. Liu, *J. Mater. Sci.* **24**, 4745–4756 (2013)
- W.W. Ma, X.T. Dong, J.X. Wang, W.S. Yu, G.X. Liu, *J. Mater. Sci.* **48**, 2557–2565 (2013)
- X. Zhou, J. Shen, Y. Wang, Z. Feng, R. Wang, L. Li, S. Jiang, X. Luo, *J. Am. Ceram. Soc.* **99**, 2300–2305 (2016)
- G.C. Zhu, F.B. Li, M.G. Xiao, *Trans. Nonferrous Met. Soc. China* **13**, 1454–1458 (2003)